Liquid Crystals
Publication details, including instructions for authors and subscription information:
http://www.informaworld.com/smpp/title~content=t713926090

Structure of surface-stabilized antiferroelectric liquid crystals cells

J. Sabater[a]; J. M. Otón[a]
[a] Dept. Tecnología Fotónica, ETSI Telecommunicatión, Ciudad Universitaria, Madrid, Spain

To cite this Article Sabater, J. and Otón, J. M.(1996) 'Structure of surface-stabilized antiferroelectric liquid crystals cells', Liquid Crystals, 21: 3, 397 — 413
To link to this Article: DOI: 10.1080/02678299608032849
URL: http://dx.doi.org/10.1080/02678299608032849

LIQUID CRYSTALS, 1996, VOL. 21, NO. 3, 397–413

Structure of surface-stabilized antiferroelectric liquid crystals cells

by J. SABATER and J. M. OTÓN*
Dept. Tecnología Fotónica, ETSI Telecommunicación, Ciudad Universitaria, E-28040 Madrid, Spain

(*Received 22 March 1996; accepted 22 April 1996*)

A comprehensive expression describing the director profile and energy parameters of surface-stabilized antiferroelectric liquid crystals has been derived. The expression is based on a previously developed ferroelectric liquid crystal model in which two contiguous smectic layers have been simultaneously computed. The antiferroelectric behaviour is mathematically described as an additional energy term relating these layers to each other through a coupling constant. The new energy term gives significant differences in the material behaviour, as compared with the ferroelectric phase. Electrically induced antiferroelectric–ferroelectric phase transitions are predicted as well. The effect of every term on the general expression has been analyzed. Comparisons with ferroelectric results are also included.

1. Introduction

The bistable fast switching shown by surface-stabilized ferroelectric liquid crystals [1] has attracted interest from both the basic and practical point of view [2], for these materials could be employed for manufacturing electro-optical devices provided with intrinsic memory. This feature is specially important in multiplexed displays, where the liquid crystal's intrinsic memory avoids the use of complicated external electronics, such as active matrices of thin film transistors. Soon it was realized that bistability, being itself a clear advantage for multiplex driving, precludes however the generation of intermediate optical transmission states, i.e. grey levels, which are necessary for many display applications including TV and computer screens.

An antiferroelectric liquid crystal (AFLC) phase [3] was discovered as a result of the anomalous tristable switching [4] shown by some ferroelectric liquid crystals. Surface-stabilized AFLCs can be electrically switched to two opposite ferroelectric states [5]. The interest in these materials has been enhanced by the recent demonstration [6] of grey levels in an AFLC display with crossed polarizers oriented with the antiferroelectric director (i.e. the rubbing direction). Although some simplified expressions have been proposed [7], an accurate mechanism describing the generation of grey levels has not yet been presented. This is due in part to the lack of a comprehensive model describing the director profile along the AFLC cell, and the relative contributions of the different energy terms to the overall energy of the system. Surface-stabilized structures are usually far more complex than originally proposed [8]. The bookshelf structure of smectic layers is seldom obtained, symmetric and asymmetric chevron structures [9] constituting the most usual configuration. This complexity has so far permitted only a limited understanding of their physical properties. In recent work [10], a non-simplified expression for surface-stabilized ferroelectric liquid crystals was presented. A single smectic layer was used in this case for solving the system.

In this work, a general expression for surface-stabilized AFLCs is presented and solved. As in the previous work, no simplifications have been introduced, except in those cases where non-relevant improvements in accuracy lead the complexity of the expressions beyond practical computation analysis. In the solution of an AFLC case, two contiguous layers must be considered, since their profiles are inter-related through a coupling energy. This interlayer coupling, which ultimately dictates the formation of either ferroelectric or antiferroelectric phases, will be extensively analyzed in this work.

2. System geometry

The geometrical reference system shown in figure 1 is employed. A chevron structure is assumed. The chevron 'kink' is rounded up, i.e. it is not a discontinuity. The angles used for defining the basic unit vectors are also included. As the antiferroelectric model needs two layers for its formulation, every vector related to the position of a molecule is defined twice: one for each layer. The subscript i, whose possible values are 1 and 2, is used

*Author for correspondence.

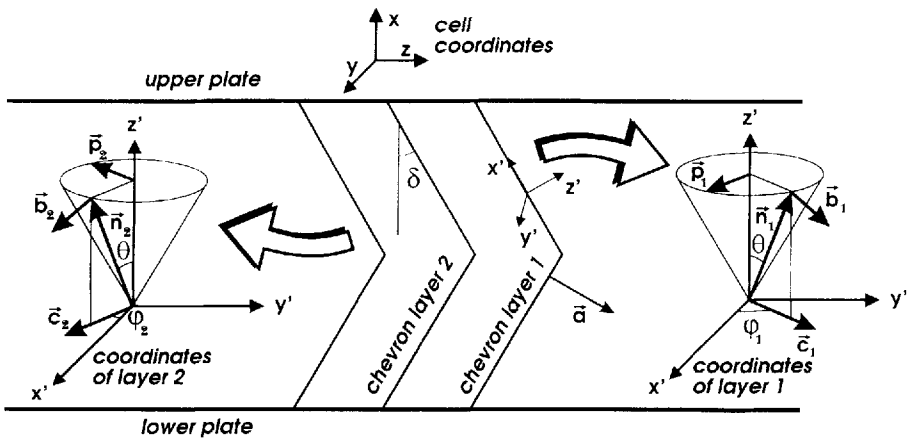

Figure 1. System geometry.

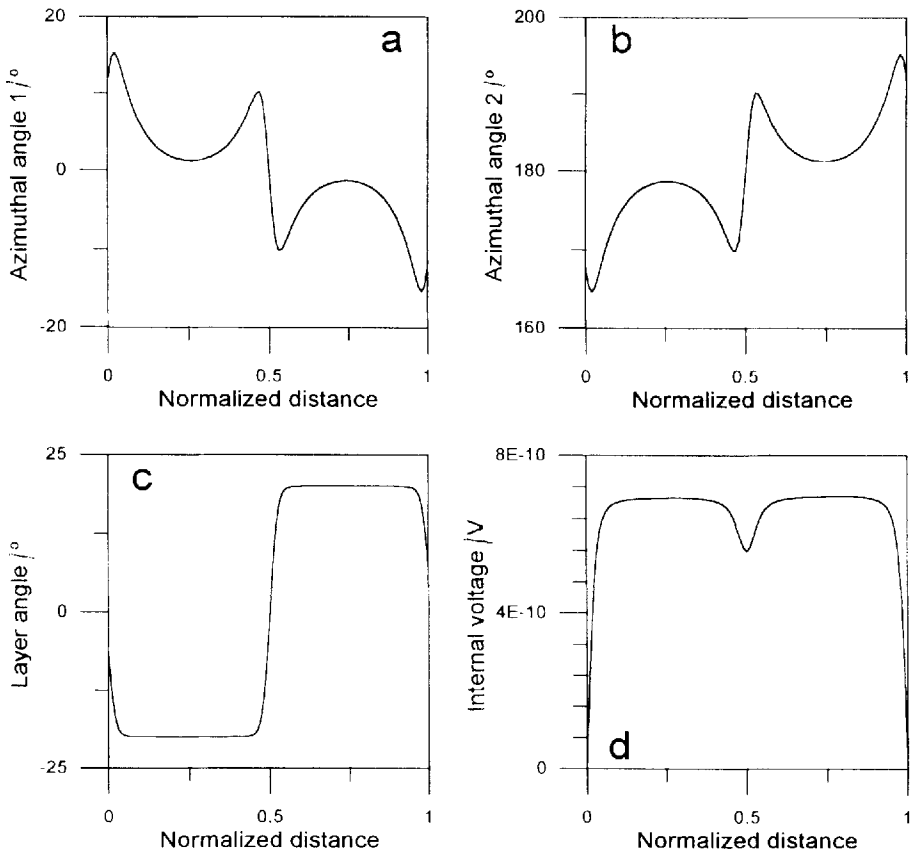

Figure 2. Typical solution for an AFLC system. (*a*) and (*b*) are both for azimuthal angles; (*c*) is for the layer angle; (*d*) is for the internal voltage. The symmetry of the functions is determined by the set of parameters.

for referring to each layer. The following unit vectors are defined:

- **a** perpendicular to the smectic layer,
- $\mathbf{c}_i$ director projection on both smectic layers,
- $\mathbf{n}_i$ molecular directors, and tertiary axes of the dielectric tensors,
- $\mathbf{p}_i$ secondary axes of the dielectric tensors,
- $\mathbf{b}_i$ primary axes of the dielectric tensors.

These vectors are expressed in terms of four angles: φ_1, φ_2, δ and θ. The first two are the azimuthal angles of the directors in each layer; the third is the layer angle and the fourth is the molecular tilt angle. The expressions

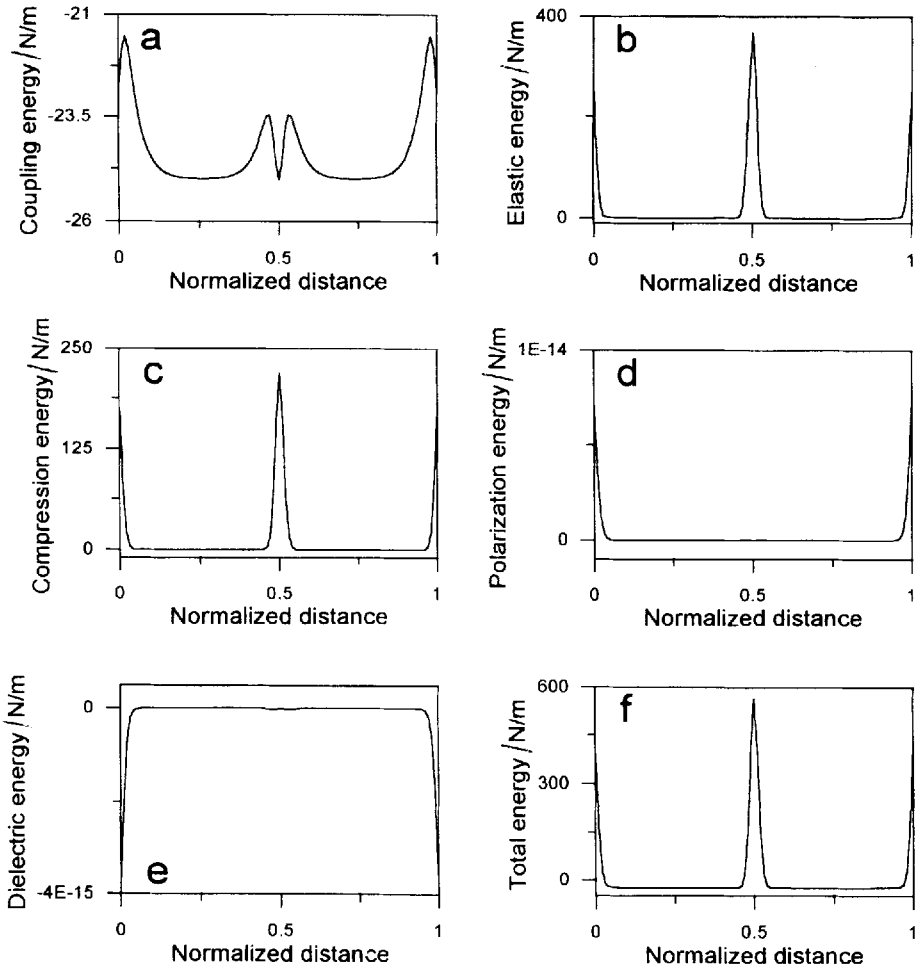

Figure 3. Energy densities in the AFLC cell. (*a*) is the interlayer coupling energy; (*b*) is the elastic energy density; (*c*) is the layer compression density; (*d*) and (*e*) show the interaction of the electric field with the spontaneous polarization and the dielectric tensor, respectively; (*f*) shows the sum of the previous contributions. Note that the energy concentrates on the surfaces and on the chevron kink.

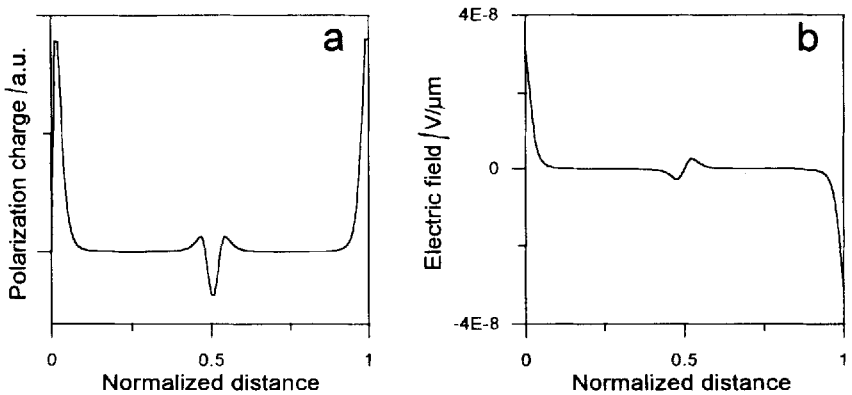

Figure 4. Electric parameters in the same AFLC cell as in figure 3. (*a*) polarization charge along the cell; (*b*) internal electric field.

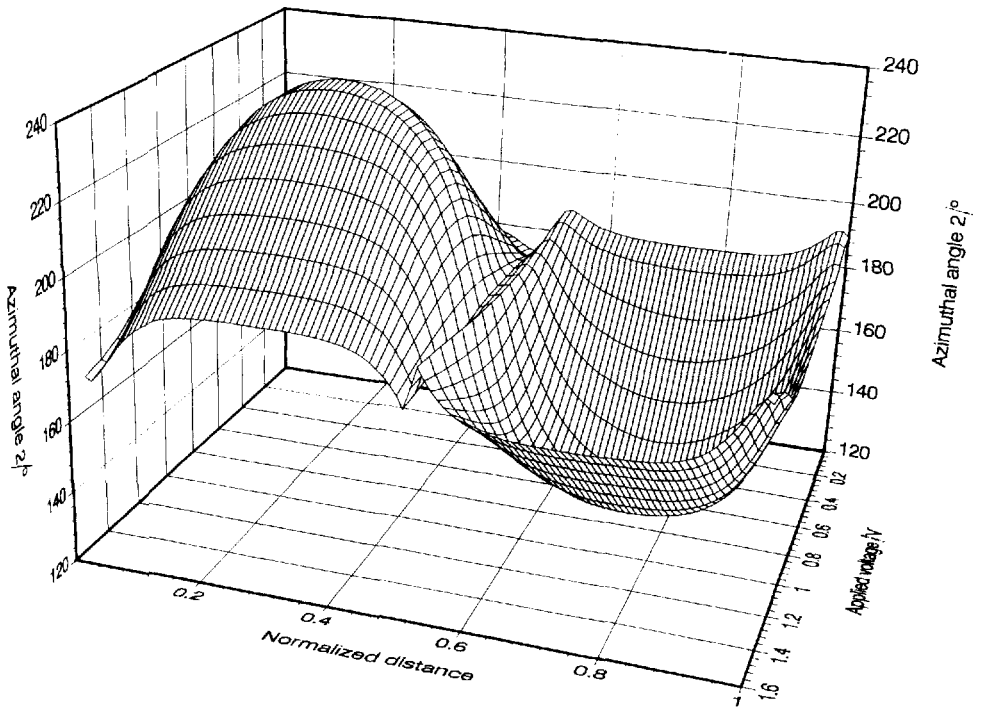

Figure 5. Evolution of the equilibrium profile of already switched molecules with increasing applied voltage. The central fluctuation is due to interlayer coupling.

for these vectors are:

$$\mathbf{a} = [\sin\delta, 0, \cos\delta] \tag{1}$$

$$\mathbf{n}_i = [-\sin\theta\sin\varphi_i\cos\delta + \cos\theta\sin\delta, \sin\theta\cos\varphi_i, \sin\theta\sin\varphi_i\sin\delta + \cos\theta\cos\delta] \tag{2}$$

$$\mathbf{p}_i = [-\cos\varphi_i\cos\delta, -\sin\varphi_i, \cos\varphi_i\sin\delta] \tag{3}$$

$$\mathbf{b}_i = [-\cos\theta\sin\varphi_i\cos\delta - \sin\theta\sin\delta, \cos\theta\cos\varphi_i, \cos\theta\sin\varphi_i\sin\delta - \sin\theta\cos\delta] \tag{4}$$

$$\mathbf{c}_i = [-\sin\varphi_i\cos\delta, \cos\varphi_i, \sin\varphi_i\sin\delta] \tag{5}$$

Only variations along the normal to the cell plates, i.e. along the x-axis, are studied. Moreover, the molecular tilt θ is assumed to be constant. This is required to keep the mathematical system within reasonable computation limits. Moreover, actual variations of the molecular tilt have only a small influence on the accuracy of the system resolution. Indeed, tilt variations are significant only at the cell surfaces—where layers maintain the S_A spacing and therefore θ equals zero—and at the chevron 'kink' where a rapid variation of the layer angle is present, unless a layer discontinuity is accepted. The thickness of these regions is very small compared to the cell thickness. Tilt variations affect limited areas of the compression energy density, and have negligible effects on the interlayer coupling.

3. Energy description

Director profiles are calculated by minimizing the total system energy. In a surface-stabilized AFLC, this energy is the sum of four contributions: antiferroelectric coupling energy, bulk elastic energy, volume electric energy, and surface energy. The last three contributions are similar to the homologous terms in surface-stabilized ferroelectric liquid crystals. External voltages applied to the system, if any, are included in the volume electric energy contribution.

The coupling energy relates the relative orientation of the directors in two contiguous layers. The term includes a coupling constant whose sign determines whether the material tends to be ferroelectric or antiferroelectric in the absence of external fields.

The elastic energy calculation is very complex [11]. Expressions involving more than thirty elastic constants can be found [12]. These expressions cannot be reliably computed; moreover, no experimental values of these constants for any material are known. Physically meaningful simplified expressions of elastic energy contributions have been proposed [13].

Evaluation of volume electric energy is relatively

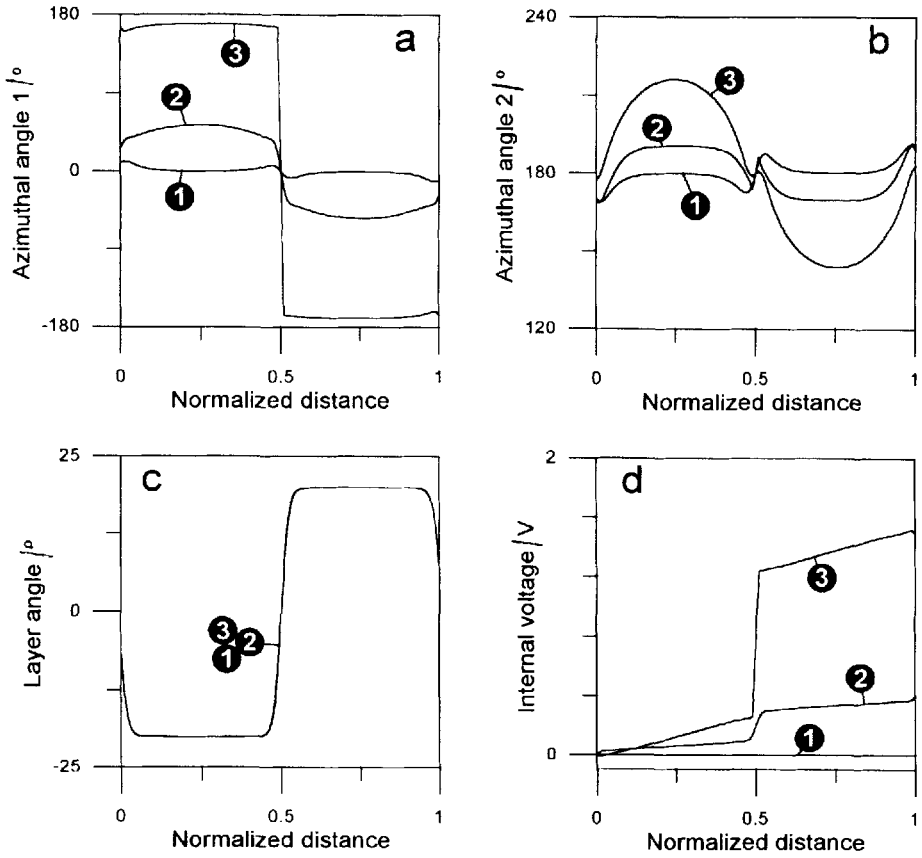

Figure 6. Complete solutions for an AFLC cell for different applied voltages: $V_1 = 0\,V$, $V_2 = 0{\cdot}4\,V$ and $V_3 = 1{\cdot}5\,V$. (*a*) shows switching of the first azimuthal angle; (*b*) shows fluctuation of the second azimuthal angle; in (*c*), there is no layer angle profile variation. The abrupt change in the internal voltage profiles represented in (*d*) is a characteristic of AFLCs.

simple. An exact expression depending on four constants can be formulated [14]. These constants are related to the three components of the dielectric tensor and the spontaneous polarization, respectively [15].

Many expressions for surface energy have been proposed [16–18]. Accurate expressions must take into account the molecular pretilt at the surfaces, the presence and angular variation of two (symmetric or asymmetric) minima, and the height of the potential barrier between these minima. The formulation of each surface (up and down) must be separately done allowing the surface energy to be different at each plate.

3.1. *Antiferroelectric coupling energy*

This energy defines the coupling found between adjacent smectic layers. There are two possibilities: in an ideal ferroelectric, the energy minimizes when the molecules of contiguous layers are located in the same point of the smectic cone; on the contrary in an ideal antiferroelectric, adjacent molecules tend to be diametrically opposed to each other. The expression of this energy, f_c, in a two layers model [19] is:

$$f_c = K_p(P_1 \cdot P_2) = K_p P_s^2 \cos(\varphi_1 - \varphi_2) \qquad (6)$$

The coupling constant K_p determines whether the material is ferroelectric ($K_p < 0$) or antiferroelectric ($K_p > 0$). As seen in equation (6), f_c is independent of the molecular tilt θ.

3.2. *Bulk elastic energy*

The formulation proposed by Nakagawa [17] is used. The vectorial formulation of the bulk elastic energy density, f_{elas}, is:

$$f_{elas} = \frac{A}{2}(\nabla \cdot \mathbf{a})^2 + \frac{B}{2}\sum_{i=1}^{2}[(\nabla \cdot \mathbf{c}_i)^2 + (\nabla \times \mathbf{c}_i)^2] - C\sum_{i=1}^{2}(\nabla \cdot \mathbf{a})(\nabla \cdot \mathbf{c}_i) - D\sum_{i=1}^{2}(\mathbf{c}_i \cdot \nabla \times \mathbf{c}_i) + \frac{L}{2}\left(\frac{\cos\delta}{\cos\delta_0} - 1\right)^2 \qquad (7)$$

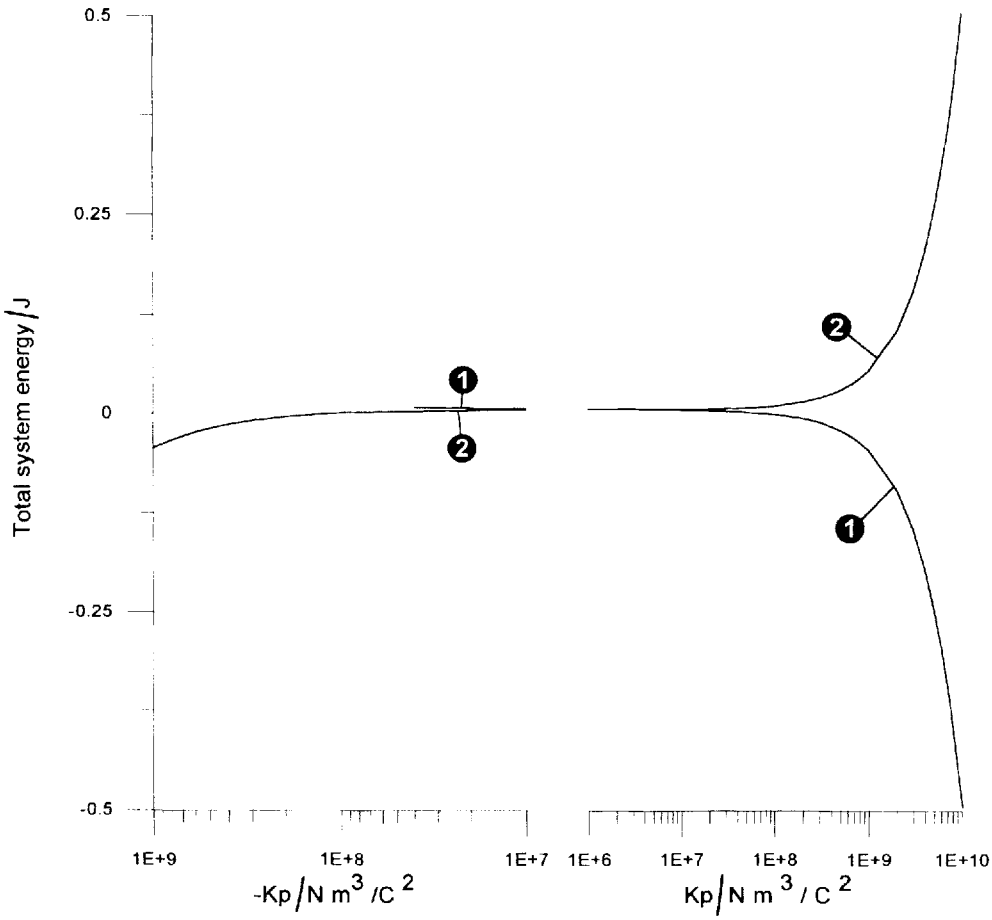

Figure 7. Total system energy as a function of K_p for antiferroelectric (1) and ferroelectric (2) configurations. No difference is found in the central part of the x-axis. The ferroelectric configuration is more stable if $K_p < 0$, and the antiferroelectric configuration is more stable if $K_p > 0$.

This equation is similar to the corresponding energy of a ferroelectric, but some terms have to be duplicated here to account for both smectic layers. The A-term describes the layer deformation energy, the B-term is the energy of molecular rotation inside the layer, the C-term relates the two previous terms, the D-term is the chiral energy and the L-term is the layer compression energy. A, B, C, and D are elastic constants, L is the compression modulus and δ_0 is the equilibrium layer tilt angle. This formulation of the compression energy assumes a constant molecular tilt angle through the cell. If tilt angle variations were to be considered, the L-term would be substituted; the new expression would then take into account the most favourable θ value and the δ–θ coupling at every point.

Substituting the expressions of the vectors in equation (7), the following expression is obtained:

$$f_{\text{elas}} = \left(\frac{A}{2}\cos^2\delta + \frac{B}{2}\sum_{i=1}^{2}\sin^2\varphi_i - \frac{C}{2}\sin 2\delta \sum_{i=1}^{2}\sin\varphi_i\right)\delta_x^2 + \frac{B}{2}\sum_{i=1}^{2}\varphi_{i,x}^2 + C\cos^2\delta\left(\sum_{i=1}^{2}\cos\varphi_i\varphi_{i,x}\right)\delta_x + \frac{D}{2}\cos\delta\left(\sum_{i=1}^{2}\sin 2\varphi_i\right)\delta_x + D\sin\delta\sum_{i=1}^{2}\varphi_{i,x} + \frac{L}{2}\left(\frac{1}{\cos^2\delta} - \frac{1}{\cos^2\delta_0}\right)^2 \quad (8)$$

The subscript x means derivative with respect to x. The double subscript i,x is used in derivatives of φ_1 and φ_2.

3.3. *Electric energy*

The electric energy has two main contributions, one due to the interaction of the spontaneous polarizations

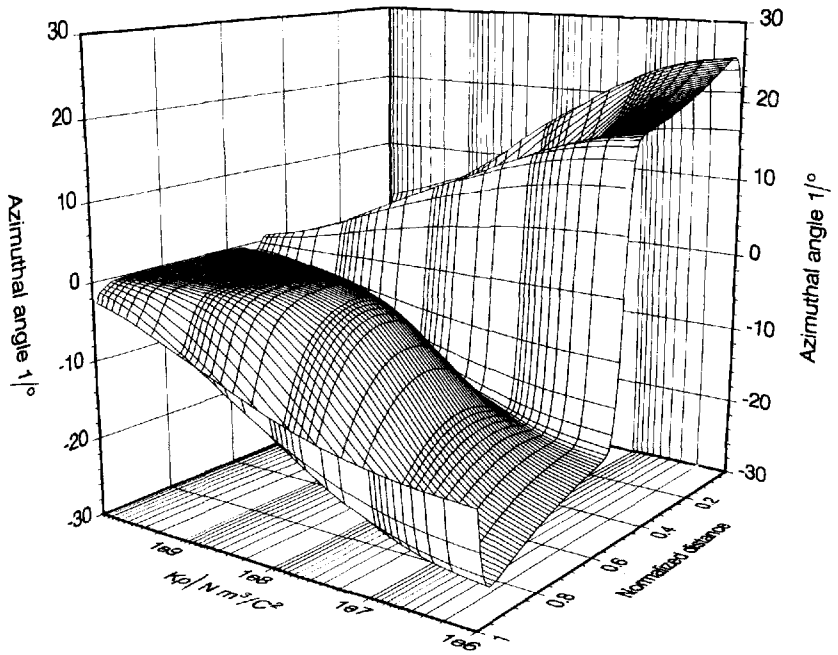

Figure 8. Evolution of the first azimuthal angle with increasing K_p. The azimuthal profiles tend to flatten as the interlayer coupling increases.

of both layers and the electric field, and the other due to the interaction of the dielectric tensors of both layers and the electric field. As the spontaneous polarization itself induces an internal voltage, these terms are non-zero even without an external applied field.

The spontaneous polarization term, f_{pol}, is:

$$f_{pol} = P_s \cos\delta \left(\sum_{i=1}^{2} \cos\varphi_i \right) V_x \tag{9}$$

where the function V is the voltage in each point of the cell.

The components of the dielectric tensors are:

$$(\varepsilon_{jk})_i = \varepsilon_1 b_j b_k + \varepsilon_2 p_j p_k + \varepsilon_3 n_j n_k \tag{10}$$

where ε_1, ε_2, and ε_3 are the tensor diagonal components. The electric field is taken to be vertical; therefore, the dielectric energy, f_{diel}, is:

$$f_{diel} = -\frac{1}{2}\varepsilon_{11} V_x^2 \tag{11}$$

Substituting ε_{11}:

$$f_{diel} = -\frac{1}{2}\sum_{i=1}^{2} [\varepsilon_1 + \delta\varepsilon \cos^2\delta \cos^2\varphi_i + \Delta\varepsilon(\cos\theta \sin\delta - \sin\theta \sin\varphi_i \cos\delta)^2] V_x^2 \tag{12}$$

where $\Delta\varepsilon$ and $\delta\varepsilon$ are the dielectric anisotropy and biaxiality, respectively, defined as:

$$\Delta\varepsilon = \varepsilon_3 - \varepsilon_1 \qquad \delta\varepsilon = \varepsilon_2 - \varepsilon_1 \tag{13}$$

3.4. *Surface energy*

The surface energy formulation from Nakagawa [17] is used. The surface energy contributions at the upper plate are f_{up1} and f_{up2} and at the lower plate are f_{dn1} and f_{dn2}. Subscripts 1 and 2 correspond to φ_1 and φ_2 respectively. The expression of this energy at each plate for each director is:

$$f_{up_i} = -g_{up}\left[c_{up} \exp\left(-\alpha \sin^2 \frac{\varphi_i - \varphi_{up}}{2} \right) + (1 - c_{up}) \exp\left(-\alpha \cos^2 \frac{\varphi_i + \varphi_{up}}{2} \right) \right] \tag{14}$$

$$f_{dn_i} = -g_{dn}\left[c_{dn} \exp\left(-\alpha \sin^2 \frac{\varphi_i - \varphi_{dn}}{2} \right) + (1 - c_{dn}) \exp\left(-\alpha \cos^2 \frac{\varphi_i + \varphi_{dn}}{2} \right) \right] \tag{15}$$

where g is the magnitude of the surface energy, c is the function symmetry at $\pi/2$, α is the slope of the potential barrier, and φ_{dn} and φ_{up} are the stable azimuthal angles at each surface, which depend on the tilt angle and the surface pretilt. This expression is obviously identical to the ferroelectric expression.

4. Euler–Lagrange equations

Once all the energies involved in the system under study are formulated, the Euler–Lagrange equations describing the minimum energy states of the system may

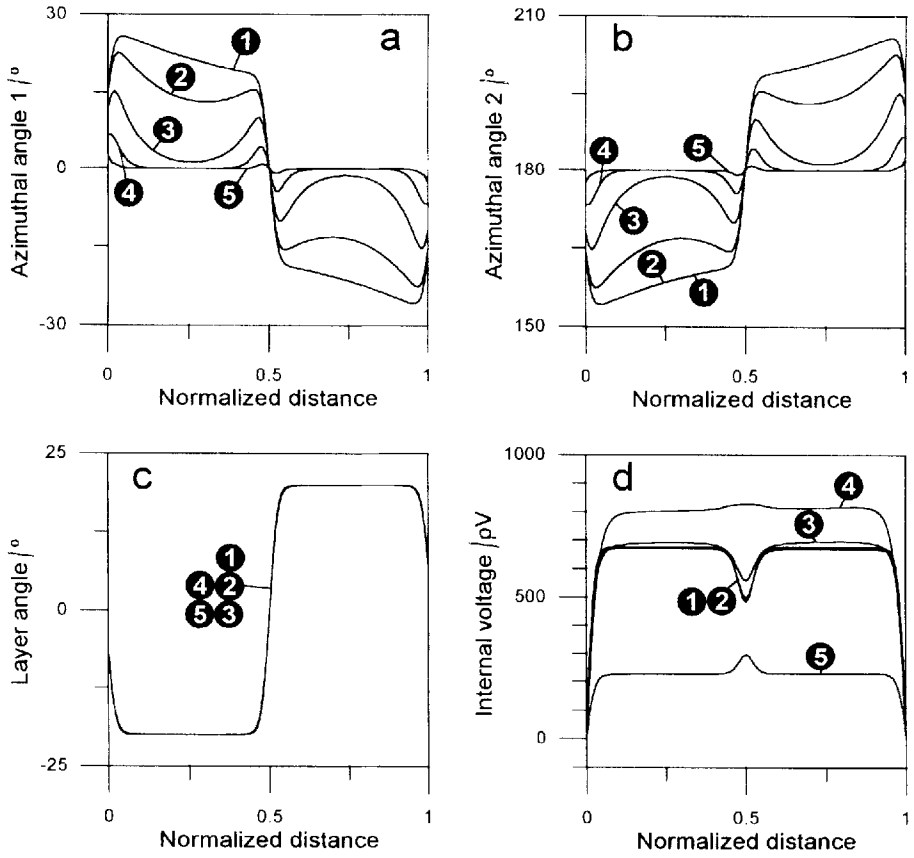

Figure 9. Complete solutions for different coupling constants: $K_{p1} = 10^6\,\mathrm{N\,m^3\,C^{-2}}$, $K_{p2} = 10^7\,\mathrm{N\,m^3\,C^{-2}}$, $K_{p3} = 10^8\,\mathrm{N\,m^3\,C^{-2}}$, $K_{p4} = 10^9\,\mathrm{N\,m^3\,C^{-2}}$ and $K_{p5} = 10^{10}\,\mathrm{N\,m^3\,C^{-2}}$. The azimuthal angles (*a*) and (*b*) flatten with increasing K_p; the layer angle distribution (*c*) remains unchanged; the internal voltage (*d*) shows a complex variation as a result of several simultaneous interactions.

be derived. The total bulk energy density, f_{vol}, is:

$$f_{vol} = f_c + f_{elas} + f_{pol} + f_{diel} \tag{16}$$

The Euler–Lagrange equations are derived in terms of four functions: φ_1, φ_2, δ and V; their expressions are:

$$\frac{\partial f_{vol}}{\partial \varphi_1} - \frac{d}{dx}\frac{\partial f_{vol}}{\partial\left(\frac{\partial \varphi_1}{\partial x}\right)} = 0 \qquad \frac{\partial f_{vol}}{\partial \varphi_2} - \frac{d}{dx}\frac{\partial f_{vol}}{\partial\left(\frac{\partial \varphi_2}{\partial x}\right)} = 0$$

$$\frac{\partial f_{vol}}{\partial \delta} - \frac{d}{dx}\frac{\partial f_{vol}}{\partial\left(\frac{\partial \delta}{\partial x}\right)} = 0 \qquad \frac{\partial f_{vol}}{\partial V} - \frac{d}{dx}\frac{\partial f_{vol}}{\partial\left(\frac{\partial V}{\partial x}\right)} = 0 \tag{17}$$

After some algebraic simplification the following coupled set of four second order differential equations is obtained:

$$\begin{aligned}
&C\cos^2\delta\sin\varphi_1\delta_x\varphi_{1,x} - B\varphi_{1,xx} \\
&\quad + (C\sin 2\delta\cos\varphi_1 + B\sin 2\varphi_1)\frac{\delta_x^2}{2} \\
&\quad - 2D\cos\delta\sin^2\varphi_1\delta_x - C\cos^2\delta\cos\varphi_1\delta_{xx} \\
&\quad - P_s\sin\varphi_1\cos\delta V_x - K_p P_s^2\sin(\varphi_1 - \varphi_2) \\
&\quad + \left[\frac{\Delta\varepsilon}{4}\sin 2\theta\sin 2\delta\cos\varphi_1\right. \\
&\quad \left. + \frac{(\delta\varepsilon - \Delta\varepsilon\sin^2\theta)}{2}\cos^2\delta\sin 2\varphi_1\right] V_x^2 = 0
\end{aligned} \tag{18}$$

$$\begin{aligned}
&C\cos^2\delta\sin\varphi_2\delta_x\varphi_{2,x} - B\varphi_{2,xx} \\
&\quad + (C\sin 2\delta\cos\varphi_2 + B\sin 2\varphi_2)\frac{\delta_x^2}{2} \\
&\quad - 2D\cos\delta\sin^2\varphi_2\delta_x - C\cos^2\delta\cos\varphi_2\delta_{xx} \\
&\quad - P_s\sin\varphi_2\cos\delta V_x + K_p P_s^2\sin(\varphi_1 - \varphi_2) \\
&\quad + \left[\frac{\Delta\varepsilon}{4}\sin 2\theta\sin 2\delta\cos\varphi_2\right. \\
&\quad \left. + \frac{(\delta\varepsilon - \Delta\varepsilon\sin^2\theta)}{2}\cos^2\delta\sin 2\varphi_2\right] V_x^2 = 0
\end{aligned} \tag{19}$$

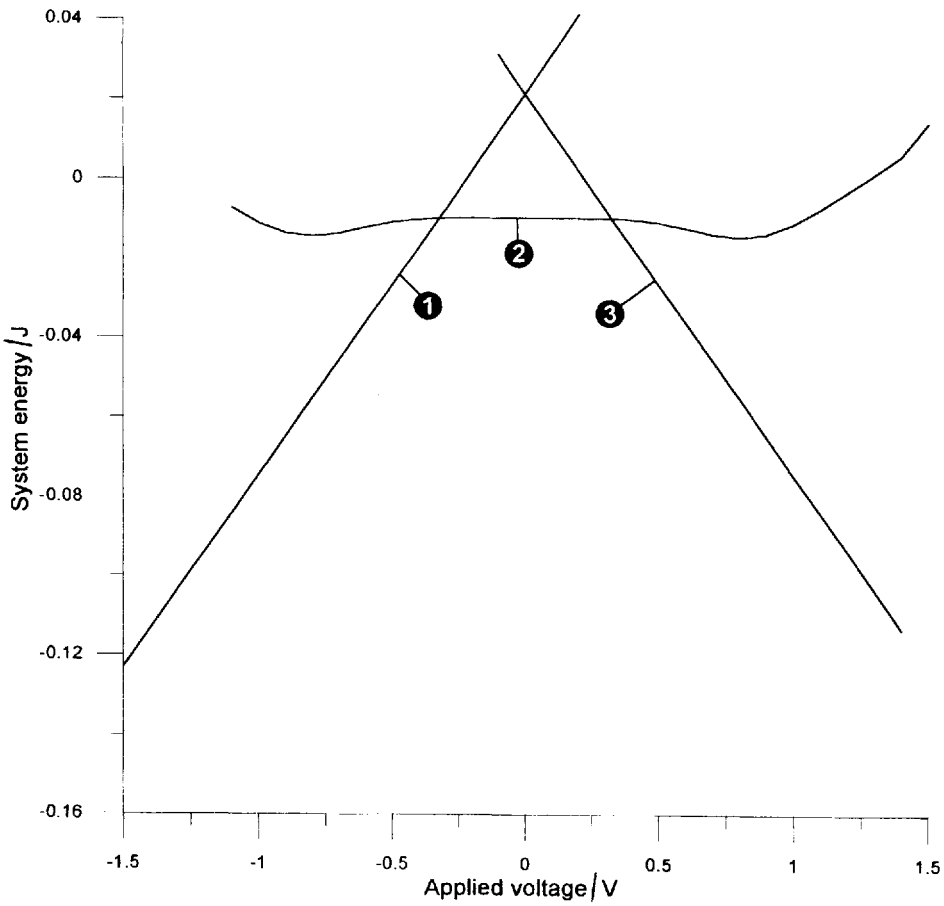

Figure 10. Total system energy as a function of applied voltage for three configurations: ferroelectric UP (1), antiferroelectric (2) and ferroelectric DN (3). The AFLC phase is more stable at low voltage. Beyond two definite thresholds, the ferroelectric phase becomes more stable.

$$\frac{\sin 2\delta}{2}\left(\Delta\varepsilon \sin 2\theta \sum_{i=1}^{2} \sin\varphi_i + (\delta\varepsilon - \Delta\varepsilon \sin^2\theta) \sum_{i=1}^{2} \cos^2\varphi_i\right) \times V_x^2 - P_s \sin\delta \left(\sum_{i=1}^{2} \cos\varphi_i\right) V_x + C\cos^2\delta \left(\sum_{i=1}^{2} \sin\varphi_i \varphi_{i,x}^2 - \sum_{i=1}^{2} \cos\varphi_i \varphi_{i,xx}\right) + \left(2C\cos 2\delta \sum_{i=1}^{2} \sin\varphi_i + A\sin 2\delta\right)\delta_x^2 + \left(\sum_{i=1}^{2} (2C\sin 2\delta\cos\varphi_i - B\sin 2\varphi_i)\varphi_{i,x}\right)\delta_x + 2D\cos\delta \sum_{i=1}^{2} (\sin^2\varphi_i \varphi_{i,x}) + \frac{D}{2}\sin\delta\left(\sum_{i=1}^{2} \sin 2\varphi_i\right)\delta_x + \left(-A\cos^2\delta - B\sum_{i=1}^{2} \sin^2\varphi_i + C\sin 2\delta \sum_{i=1}^{2} \sin\varphi_i\right)\delta_{xx} + 2\frac{L(\cos^2\delta_0 - \cos^2\delta)}{\cos^4\delta\cos^2\delta_0}\tan\delta = 0 \quad (20)$$

$$P_5 \sum_{i=1}^{2} \sin\varphi_i \cos\delta\varphi_{i,x} + P_s \sum_{i=1}^{2} \cos\varphi_i \sin\delta\,\delta_x + \sum_{i=1}^{2}\left((\Delta\varepsilon \sin^2\theta - \delta\varepsilon)\cos^2\delta \sin^2\varphi_i - \frac{\Delta\varepsilon}{2}\sin 2\delta \sin 2\theta \cos\varphi_i\right)\varphi_{i,x} V_x + \sin 2\delta\left((\Delta\varepsilon \sin^2\theta - \delta\varepsilon)\sum_{i=1}^{2} \cos^2\varphi_i - \Delta\varepsilon \sin 2\theta \sum_{i=1}^{2} \sin\varphi_i + 2\Delta\varepsilon\cos 2\theta\right)\delta_x V_x + \left[2\varepsilon_1 - (\Delta\varepsilon \sin^2\theta - \delta\varepsilon)\cos^2\delta \sum_{i=1}^{2} \cos^2\varphi_i - \frac{\Delta\varepsilon}{2}\sin 2\theta \sin 2\delta \sum_{i=1}^{2} \sin\varphi_i + 2\Delta\varepsilon(\cos^2\theta + \cos^2\delta - 2\cos^2\theta\cos^2\delta)\right] V_{xx} = 0 \quad (21)$$

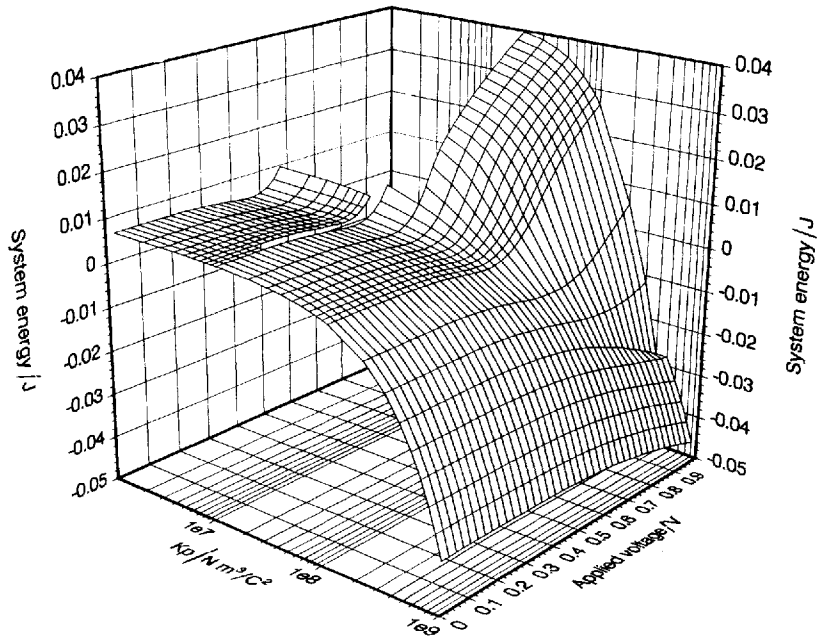

Figure 11. Total system energy as a function of K_p and of the applied voltage for an AFLC configuration. The grid points are not shown where the configuration is not stable.

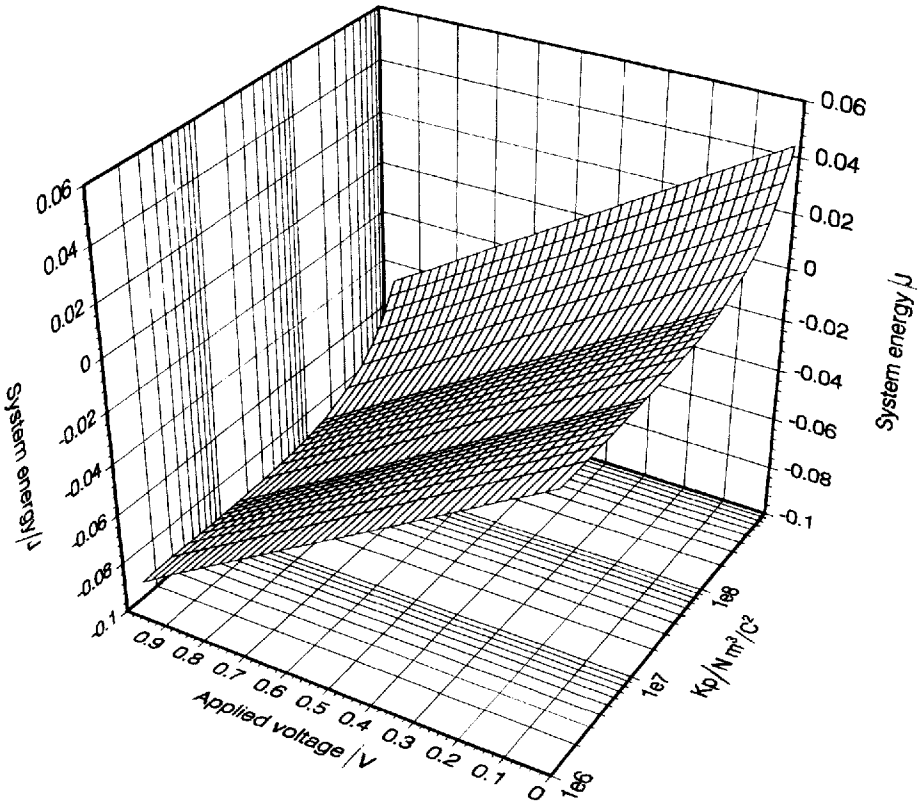

Figure 12. Total system energy as a function of K_p and of the applied voltage for a ferroelectric configuration.

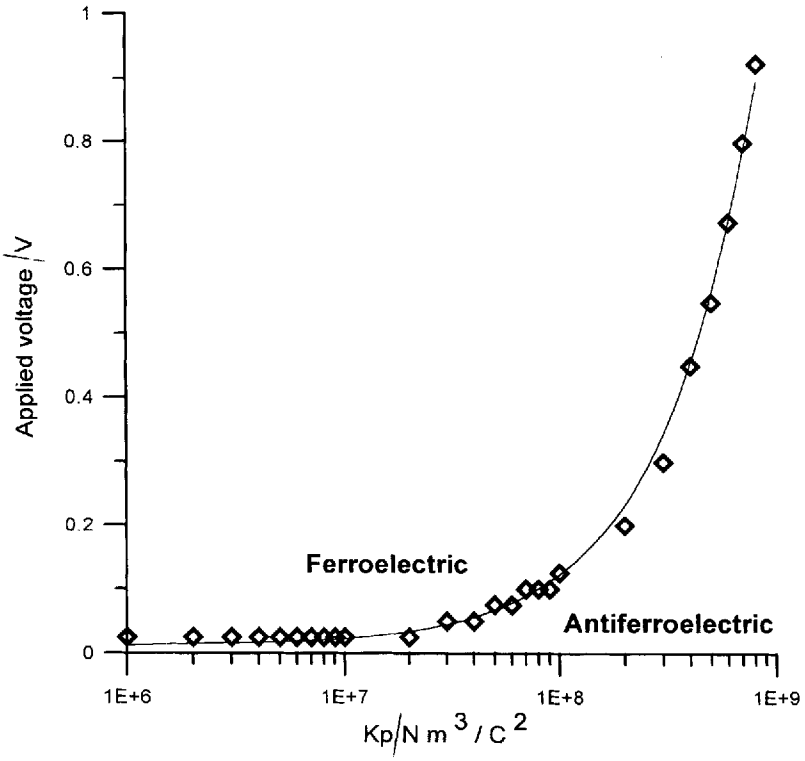

Figure 13. Phase diagram for a material exhibiting an AFLC phase as a function of K_p and of the applied voltage.

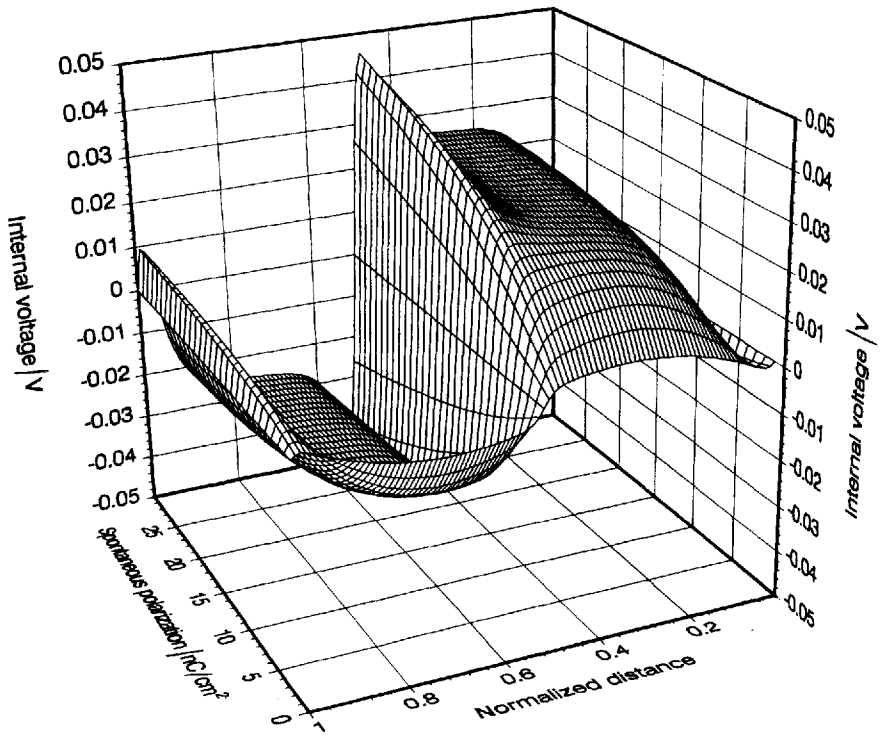

Figure 14. Evolution of the internal voltage in a ferroelectric with increasing spontaneous polarization.

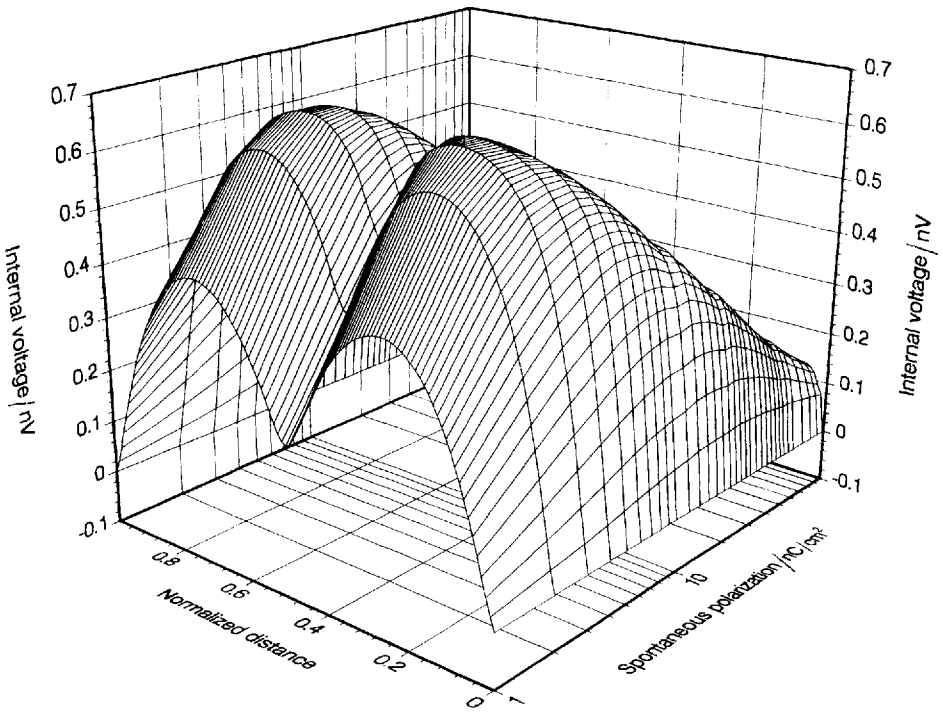

Figure 15. Evolution of the internal voltage in an antiferroelectric with increasing spontaneous polarization. The graph shows the low P_s part of the surface.

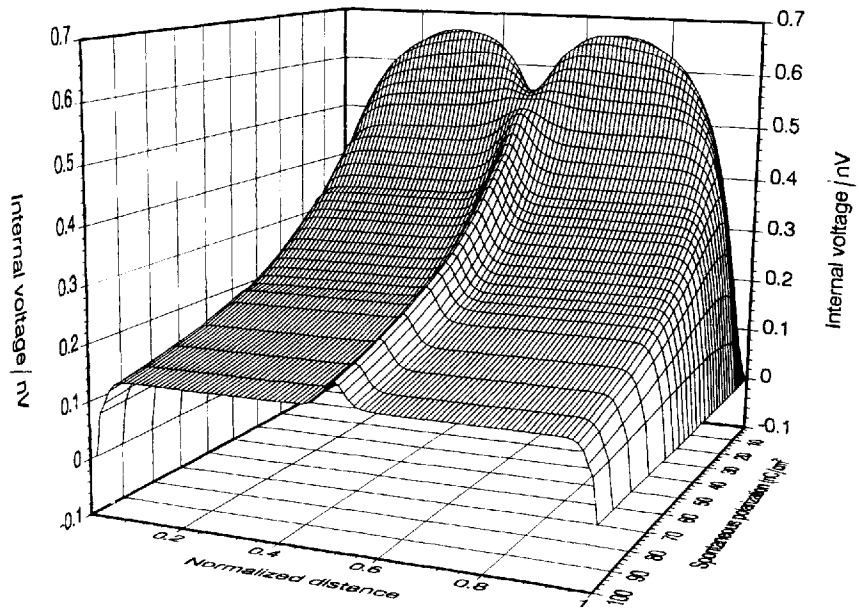

Figure 16. Evolution of the internal voltage in an antiferroelectric with increasing spontaneous polarization. The graph shows the high P_s part of the surface.

5. Boundary conditions

Finally, appropriate boundary conditions for φ_1, φ_2, δ, and V must be formulated. Boundary conditions for voltage are fixed by the voltage difference between the plates. The boundary values for δ at the surfaces are taken equal to the molecular pretilt. Finally, boundary conditions for the azimuthal angles φ_1 and φ_2 are derived from the interaction of surface energy, f_{surf}, and volume

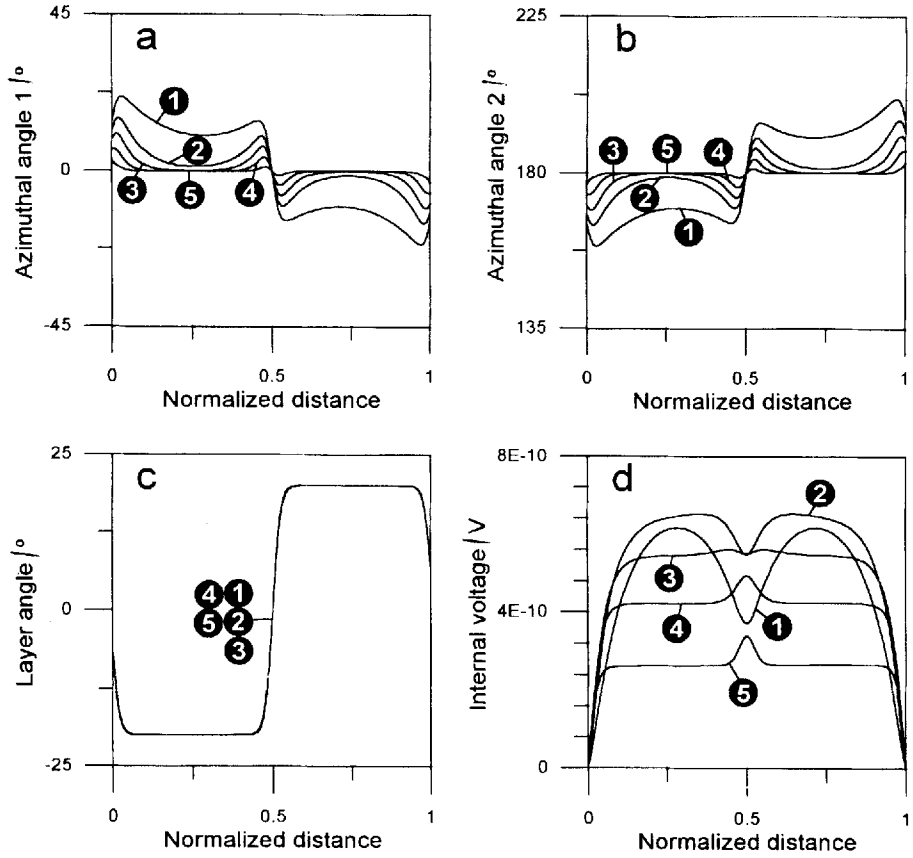

Figure 17. Complete solutions for AFLCs with different spontaneous polarizations: $P_{s1} = 2\,\mathrm{nC\,cm^{-2}}$, $P_{s2} = 5\,\mathrm{nC\,cm^{-2}}$, $P_{s3} = 9\,\mathrm{nC\,cm^{-2}}$, $P_{s4} = 17\,\mathrm{nC\,cm^{-2}}$ and $P_{s5} = 40\,\mathrm{nC\,cm^{-2}}$. The azimuthal angles (*a*) and (*b*) get flatter as the spontaneous polarization grows; the layer angle distribution (*c*) remains unchanged; the internal voltage (*d*) shows a complex variation as seen in figures 15 and 16.

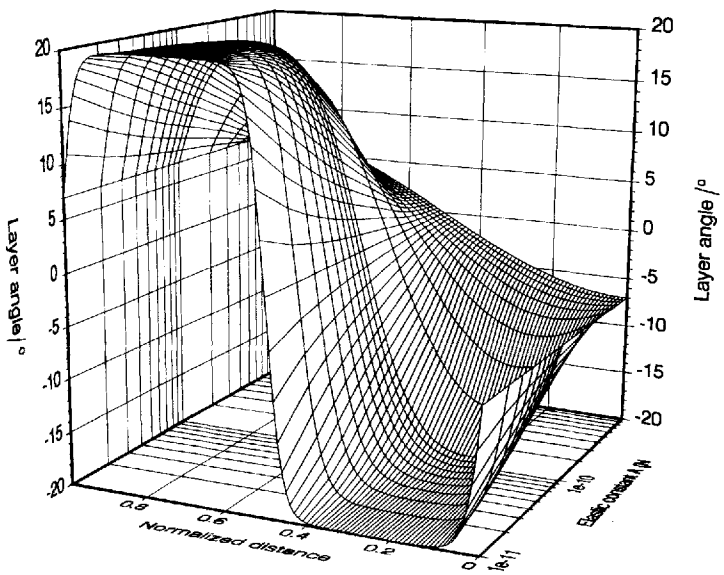

Figure 18. Evolution of the AFLC laye angle distribution as the elastic constant A increases.

energy density:

$$\frac{\partial f_{vol}}{\partial \varphi_{i,x}} + \frac{\partial f_{surf}}{\partial \varphi_i} = 0 \qquad (22)$$

Opposite signs apply to each plate. Top plate boundary conditions for both azimuthal angles ($i = 1, 2$) are:

$$-\frac{g_{up}}{2}\left[-\frac{c_{up}\alpha}{2}\sin(\varphi_i - \varphi_{up})\exp\left(-\alpha\sin^2\frac{\varphi_i - \varphi_{up}}{2}\right)\right.$$
$$+\frac{(1-c_{up})\alpha}{2}\sin(\varphi_i + \varphi_{up})$$
$$\left.\times\exp\left(-\alpha\cos^2\frac{\varphi_i + \varphi_{up}}{2}\right)\right]$$
$$+ C\cos^2\delta\cos\varphi_i\delta_x + D\sin\delta + B\varphi_{i,x} = 0 \qquad (23)$$

whereas bottom plate conditions are:

$$-\frac{g_{dn}}{2}\left[-\frac{c_{dn}\alpha}{2}\sin(\varphi_i - \varphi_{dn})\exp\left(-\alpha\sin^2\frac{\varphi_i - \varphi_{dn}}{2}\right)\right.$$
$$+\frac{(1-c_{dn})\alpha}{2}\sin(\varphi_i + \varphi_{dn})$$
$$\left.\times\exp\left(-\alpha\cos^2\frac{\varphi_i + \varphi_{dn}}{2}\right)\right]$$
$$- C\cos^2\delta\cos\varphi_i\delta_x - D\sin\delta - B\varphi_{i,x} = 0 \qquad (24)$$

6. Problem solution

The numerical resolution of the proposed coupled set of four second order differential equations with boundary conditions in both sides of the solution space has been achieved by relaxation methods [20]. In these methods, the differential equations are reduced to difference equations and a set of linear equations is obtained. The result is a grid of values of the desired functions. The grid must be dense enough for the approximations introduced when transforming differential equations into difference equations to hold. There is ultimately a trade off between the number of points taken in the grid, and the required computing resources. In this case, 100 to 300 points were needed.

Relaxation methods, although very powerful, are difficult to manage, because they usually have convergence problems for many reasons: soft boundary conditions, high number of equations and, above all, deficient initial guesses for starting the iterative process. In this work, initial guesses have been obtained from the former ferroelectric model.

7. Results and discussion

A default set of parameter values was chosen; parameter variation studies were performed keeping constant the remaining parameters. The default set is: $A = 10\,\text{pN}$; $B = 1\,\text{pN}$; $C = 1\,\text{pN}$; $D = 1\,\text{pN m}^{-1}$; $L = 25\,000\,\text{J m}^{-3}$; $P_s = 50\,\text{nC cm}^{-2}$; $\theta = 22{\cdot}5°$; $\delta_0 = 20°$; $d = 2\,\mu\text{m}$; $K_p = 100\,\text{MN m}^3\,\text{C}^{-2}$; $\Delta\varepsilon = -0{\cdot}5$; $\delta\varepsilon = 0{\cdot}2$; $\varepsilon_1 = 1{\cdot}5$; $g_{up} = g_{dn} = 50\,\mu\text{N m}^{-1}$; $c_{up} = c_{dn} = 0{\cdot}5$; $\alpha = 5$; $\varphi_{up} = 162°$; $\varphi_{dn} = 18°$. The values of the elastic constants and the compression modulus have been chosen within the ranges currently employed in the literature. The tilt and layer angles, dielectric constants, cell thickness, and surface energy constants have been selected to be similar to values used for ferroelectric liquid crystals. A moderate value of K_p has been chosen, so that it would not mask the variations of other parameters.

The effect of every parameter was studied. The most relevant results are shown below. Special attention is paid to those results which are significantly different for ferroelectrics and antiferroelectrics.

7.1. *Default set solutions*

The solution of this problem is a set of eight functions defined along the cell: φ_1, φ_2, δ and V, and their derivatives. Only the first four functions are presented. Figure 2 shows a typical solution, which corresponds to the default values used. Although only one additional term is included in the AFLC model, remarkable differences are found when comparing these functions to those obtained from the ferroelectric model. φ_1 and φ_2 tend to be opposite because of their coupling, but they do not succeed because K_p is moderate, and cannot overcome the effect of other energy contributions. On the other hand, the shape of the internal voltage (figure 2 (*d*)) is completely different: in the present case, where the surface conditions are symmetrical, the internal voltage is symmetric both in the ferroelectric and in the antiferroelectric model, but ferroelectrics give a point symmetry, whereas antiferroelectrics give a line symmetry. Moreover, the internal voltage in the absence of an external field is several orders of magnitude lower in antiferroelectrics than in ferroelectrics. The layer angle distribution (figure 2 (*c*)) is the only function that remains fairly constant from ferroelectrics to AFLCs. Variations of the layer angle near the plates are due to the surfaces. The rapid variation at the middle of the cell corresponds to chevron 'kink'. These features propagate to the remaining functions, φ_1, φ_2 , and V. All these functions are continuous nonetheless.

Starting with these basic functions it is possible to study many other aspects of the antiferroelectric cell. For instance, figure 3 shows energy density distributions and figure 4 relates to the polarization charge density and the internal electric field. It should be noted that the features of these figures would be smoothed if coupling between the layer angle and the tilt angle were allowed, i.e. if variations of the molecular tilt angle were considered.

7.2. *Profiles with applied voltage*

The behaviour of AFLC cells under an external electric field is quite different from that shown by ferroelectric cells. In a bistable ferroelectric cell with no applied field, the two stable director profiles (UP and DN) are mainly determined by the surface energy and the elastic bulk energy. If an increasing external voltage opposite to the equilibrium state adopted by the cell is applied, the director profile moves slightly away from its initial state until its configuration becomes unstable; then the cell switches. The initial situation in AFLCs is different: there are two director profiles, one for even layers and the other for odd layers. One of these profiles is UP and the other is DN; therefore, when an external voltage is applied, one half of the molecules already possesses an electrically favorable state, and only the other half of the molecules tries to switch. This leads to another difference between ferroelectrics and antiferroelectrics: switching in the ferroelectric case has to overcome mainly the surface potential barrier, but in the AFLC case it has to overcome the repulsion from the already switched molecules as well.

Some distinct intervals in the switching process can be easily identified. While the applied voltage is below a certain threshold, the combined force of the surface energy and the interlayer coupling is enough to keep the director profiles unchanged. Beyond this threshold, the molecules that lie against the external field start to rotate towards the opposite position of the cone, which is more stable. However, due to the interlayer coupling, the molecules that are already switched tend to deviate from their initial position. If the voltage is further increased, the electric energy becomes greater than the sum of the surface energy and the coupling energy; the first half of the molecules complete the switching and the second half return to their initial position.

Figure 5 shows the evolution of a layer originally oriented in the external field with increasing external voltage. The three intervals described above can be seen. Figure 6 shows the complete group of solutions for three different voltages.

7.3. *The effect of the coupling constant K_p: stability of the solutions*

The sign of K_p determines whether the material is ferroelectric or antiferroelectric. It is possible to solve the system using either type of initial solution, and then compute the total energy in both cases. The variation of the total system energy is shown in figure 7 as a function of K_p. There is an intermediate region in which $|K_p|$ is too low to affect the total energy. Therefore, there is no significant difference between the phases. Above a certain $|K_p|$ threshold, on the contrary, one of the configurations is far more stable than the other.

Using the positive semi-axis of K_p, the profile variations with increasing K_p can be studied. If K_p is very high, then φ_1 and φ_2 should be opposite in every point of the cell; if K_p is very low, then φ_1 and φ_2 are mostly

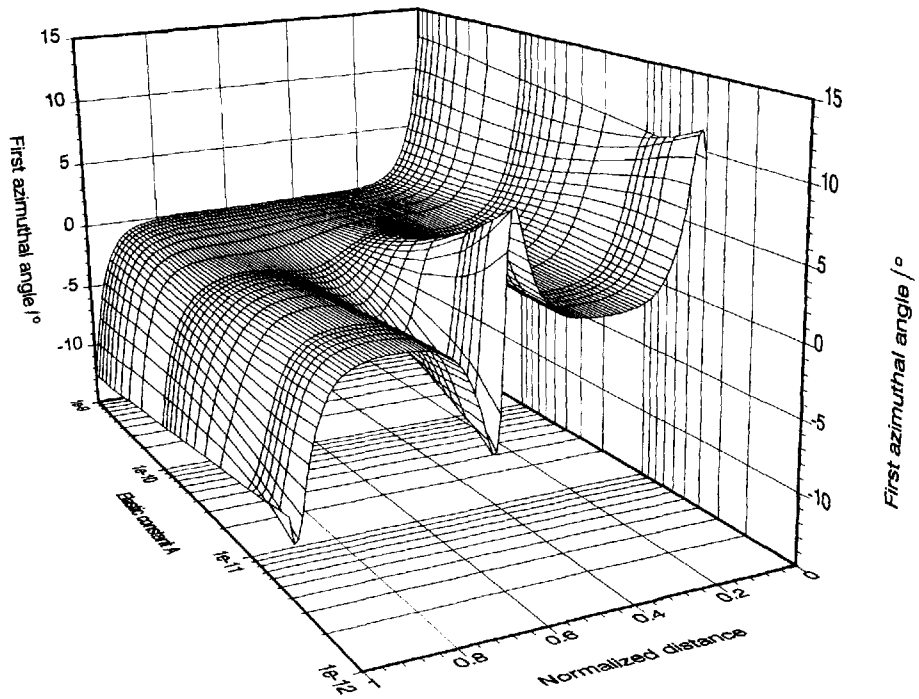

Figure 19. Evolution of one of the AFLC azimuthal angle profiles as the elastic constant A increases.

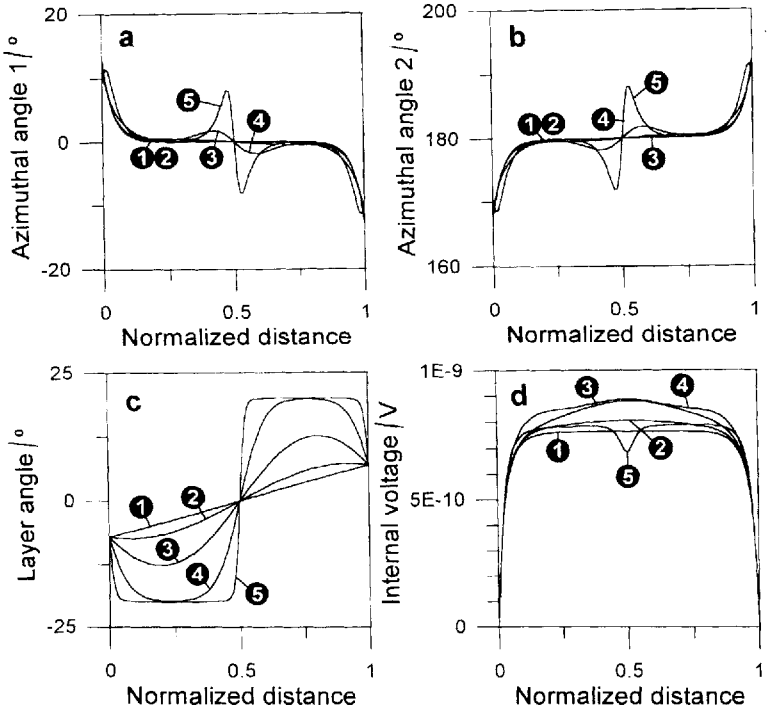

Figure 20. Complete solutions for different elastic constants: $A_1 = 9 \times 10^{-9}$ N, $A_2 = 7 \times 10^{-10}$ N, $A_3 = 3 \times 10^{-10}$ N, $A_4 = 5 \times 10^{-11}$ N, and $A_5 = 4 \times 10^{-12}$ N, The azimuthal angles (*a*) and (*b*) get flatter in the chevron kink region as A grows because the layer angle distribution (*c*) approaches a straight line and the elastic constant C tries to equate both profiles. Again, the internal voltage (*d*) has a complex evolution.

uncorrelated. Figure 8 illustrates the progressive flattening of the first azimuthal angle as K_p increases. Figure 9 shows several complete solutions for relevant K_p values.

7.4. *Relationship between K_p and the configuration stability under applied field*

An applied field may induce a phase from antiferroelectric to ferroelectric. The voltage needed for this transition heavily depends on the coupling constant K_p. Figure 10 shows the total system energy for three different configurations (ferroelectric UP, ferroelectric DN and antiferroelectric) as a function of voltage for a given K_p. There are two voltage thresholds, one for each transition (antiferroelectric to UP and antiferroelectric to DN). Because of the system's symmetry, only one needs to be analyzed. Let us focus on the transition from antiferroelectric to ferroelectric UP.

Figure 11 represents the total system energy as a function of K_p and of the applied voltage for an antiferroelectric configuration. Figure 12 is the corresponding graph for a ferroelectric UP configuration. The projection of the intersection of both surfaces defines the phase diagram of the system, and is shown in figure 13. Note that 0·025 V voltage steps have been used for this calculation. Low K_p values ($< 10^7$ N m^3 C^{-2}) lead to exceedingly low transition voltages, below the calculation resolution. Above this value, the ferroelectric and antiferroelectric areas are neatly separated.

7.5. *Spontaneous polarization variations*

The AFLC internal voltage distribution, as mentioned above, is rather different from that for the ferroelectric state. Its evolution with spontaneous polarization is also different. The zero-voltage ferroelectric internal voltage distribution has a point symmetry, and retains its initial shape as the spontaneous polarization increases. The maximum internal voltage grows steadily with the spontaneous polarization. This behaviour is depicted in figure 14. In an AFLC, neither the maximum internal voltage grows nor is the initial shape retained. The initial M-shaped internal voltage starts growing with polarization (figure 15). Above a certain value, however, it starts decreasing and the central dip changes sign (figure 16).

The spontaneous polarization affects most of the AFLC parameters, not only the internal voltage distribution. Figure 17 contains the complete group of solutions for some key values of the spontaneous polarization.

7.6. *Combined effect of elastic constant A and compression modulus L*

In the previous paragraphs, several aspects of the system that are different in ferroelectrics and antiferro-

electrics have been analyzed. There are many similar behaviours too, e.g. the role of the elastic constant A. This constant is related to the layer deformation energy and to the compression modulus. The effect of this modulus has been studied for ferroelectrics [10]. The compression modulus induces the layer angle to approach to δ_0. If A is negligible, the layer angle shape is a double step. The elastic constant A tries to minimize the variation of the layer angle; therefore, the layer angle shape for a high A is a straight line between the fixed boundary values. The intermediate stable layer angle distributions for different A values are depicted in figure 18, where L is $10^4 \mathrm{J\,m^{-3}}$. These layer angle variations are transmitted to the azimuthal angle distributions through the elastic constant C, as shown in figure 19. Figure 20 shows some complete groups of solutions for different A values.

The authors are indebted to Dr. G. Taylor from GEC (UK) for supplying AFLC test cells, and to Prof. M. Nakagawa for fruitful discussions. This work has been supported in part by the Spanish CICyT grant TIC 96-0825. JS wishes to thank CICyT for a research grant.

References

[1] CLARK, N. A., and LAGERWALL, S. T., 1980, *Appl. Phys. Lett.*, **36,** 899.
[2] OTÓN, J. M., PENA, J. M. S., SERRANO, A., and OLARTE, F., 1991, *Ferroelectrics*, **122,** 293.
[3] CHANDANI, A. D. L., GORECKA, E., OUCHI, Y., TAKEZOE, H., and FUKUDA, A., 1989, *Jpn. J. appl. Phys.*, **28,** L1265.
[4] CHANDANI, A. D. L., HAGIWARA, T., SUZUKI, Y., OUCHI, Y., TAKEZOE, H., and FUKUDA, A., 1988, *Jpn. J. appl. Phys.*, **27,** L729.
[5] FUKUDA, A., TAKANISHI, Y., ISOZAKI, T., ISHIKAWA, K., and TAKEZOE, H., 1994, *J. Mater. Chem.*, **4,** 997.
[6] OKADA, H., WATANABE, M., ONNAGAWA, H., and MIYASHITA, K., 1994, in Proceedings of the 14th International Display Research Conference, p. 491.
[7] PAUWELS, H., DE MEYERE, A., and FORNIER, J., 1995, *Mol. Cryst. liq. Cryst.* **263,** 469.
[8] HANDSCHY, M. A., and CLARK, N. A., 1984, *Ferroelectrics*, **59,** 69.
[9] MACLENNAN, J. E., CLARK, N. A., HANDSCHY, M. A., and MEADOWS, M. R., 1990, *Liq. Cryst.*, **7,** 753.
[10] SABATER, J., PENA, J. M. S., and OTÓN, J. M., 1995, *J. appl. Phys.*, **77,** 3023.
[11] DAHL, I., and LAGERWALL, S. T., 1984, *Ferroelectrics*, **58,** 215.
[12] NAKAGAWA, M., 1990, *Liq. Cryst.*, **8,** 651.
[13] NAKAGAWA, M., 1990, *Displays*, **11,** 67.
[14] DAHL, I., 1990, PhD thesis, Chalmers University of Technology, Göteborg, Sweden.
[15] JONES, J. C., RAYNES, E. P., TOWLER, M. J., and SAMBLES, J. R., 1991, *Mol. Cryst. liq. Cryst.*, **199,** 277.
[16] MACLENNAN, J. E., HANDSCHY, M. A., and CLARK, N. A., 1990, *Liq. Cryst.*, **7,** 787.
[17] NAKAGAWA, M., 1993, *Liq. Cryst.*, **14,** 1763.
[18] MEYERE, A., and DAHL, I., 1994, *Liq. Cryst.*, **17,** 397.
[19] AKAHANE, T., and OBINATA, A., 1993, *Liq. Cryst.*, **15,** 883.
[20] PRESS, W. H., TEUKOLSKY, S. A., VETTERLING, W. T., and FLANNERY, B. P., 1992, *Numerical Recipes* (Cambridge University Press).